Crystal structure of lipoate-bound lipoate ligase 1, LipL1, from *Plasmodium falciparum*

Alfredo J. Guerra [1*], Gustavo A. Afanador [1,**], Sean T. Prigge [1 #]

[1] Department of Molecular Microbiology and Immunology, Johns Hopkins Bloomberg School of Public Health, Baltimore, Maryland, USA

Address correspondence to Sean T. Prigge, sprigge2@jhu.edu

* Present address: Department of Microbiology and Immunology, University of Michigan, Ann Arbor, Michigan, USA

** Present address: Department of Biochemistry, University of Texas Southwestern Medical Center, Dallas, Texas, USA

Running Title

Malaria parasite lipoate ligase structure

Key Words

Lipoate, Malaria, Lipoylation, Lipoate ligase, Plasmodium falciparum, LipL1

Abstract

Plasmodium falciparum lipoate protein ligase 1 (*Pf*LipL1) is an ATP-dependent ligase that belongs to the biotin/lipoate A/B protein ligase family (PFAM PF03099). *Pf*LipL1 is the only known canonical lipoate ligase in *Pf* and functions as a redox switch between two lipoylation routes in the parasite mitochondrion. Here, we report the crystal structure of a deletion construct of *Pf*LipL1 (PfLipL1$_{\Delta 243\text{-}279}$) bound to lipoate, and validate the lipoylation activity of this construct in both an *in vitro* lipoylation assay and a cell based lipoylation assay.

This characterization represents the first step in understanding the redox dependence of the lipoylation mechanism in malaria parasites.

Introduction

In humans, malaria is caused by five species of Apicomplexan parasites of which *P. falciparum* is the deadliest. [1-3] The parasite lifecycle includes a sexual reproductive stage in the mosquito vector and two asexual reproductive cycles in the human host, namely the liver stage (asymptomatic) and the blood stage (symptomatic). The majority of available drugs target the blood stage;[4] although, recent findings suggest an increase of drug resistance in certain populations of parasites.[3,5-7]

The rise in drug resistance has created a necessity for new viable drug targets for malaria treatment. Lipoate metabolism is one such pathway. Lipoate is an organosulfur cofactor for a small number of enzymes that are essential for malaria parasite survival.[8,9] *P. falciparum* has two distinct organelles that contain independent pathways for lipoate metabolism.[8,10] The apicoplast, a non-photosynthetic plastid organelle, contains a biosynthetic pathway that is dispensable in the blood stage but is essential for progression from the liver to the blood stage.[10-12] In contrast to the apicoplast, the mitochondrion relies exclusively on lipoate scavenged from the host red blood cell and this pathway is essential for both the liver and blood stages.[8,12,13] Treatment with lipoate analogs, 8-bromooctanoate or 6,8-dichlorooctanoate, results in parasite growth inhibition likely due to reduced substrate lipoylation.[8,14]

There are three lipoylated enzymes in the parasite mitochondrion: the E2 component of the branched chain a-ketoacid dehydrogenase complex (BCDH, PF3D7_0303700), the E2 component of the α-ketoglutarate dehydrogenase complex (KDH, PF3D7_1320800), and the H-

protein of the glycine cleavage system (PF3D7_1132900).[9,14,15] The lipoylation of these three proteins occurs via a complex mechanism that involves two enzymes, *Pf*LipL1 (PF3D7_1314600) and *Pf*LipL2 (PF3D7_0923600). *Pf*LipL1 has been shown to be the only canonical lipoate ligase and is solely responsible for lipoylation of the H-protein – a reaction that only occurs when lipoate is in the oxidized ring form.[14] The lipoylation of BDCH and KDH requires both *Pf*LipL1 and *Pf*LipL2 as well as fully reduced lipoate (dihydrolipoate).[14] Although the mechanistic implications of redox dependence in the parasite remain unclear, *Pf*LipL1 is the switch that senses the oxidation state of lipoate and determines which downstream enzymes will be lipoylated.[16] As a first step in understanding of the molecular determinants of lipoylation activity and redox sensing in *Pf*LipL1 we determined the structure of lipoate-bound *Pf*LipL1 $_{\Delta 243\text{-}279}$.

Materials and Methods

Plasmid construction

Plasmid pMALcHT-*Pf*LipL1[14] was mutated to generate pMALcHT-*Pf*LipL1$_{\Delta 259\text{-}269}$, pMALcHT-*Pf*LipL1$_{\Delta 254\text{-}274}$, and pMALcHT-*Pf*LipL1$_{\Delta 249\text{-}279}$ using the primers listed in Table S1. Mutating the pMALcHT-*Pf*LipL1$_{\Delta 249\text{-}279}$ plasmid using the primers listed in Table S1 then generated the plasmid pMALcHT-*Pf*LipL1$_{\Delta 243\text{-}279}$. The pMALcHT plasmid encodes a maltose binding protein (MBP) followed by a linker region composed of a tobacco etch virus (TEV) protease cut site and a six histidine affinity tag.[17]

Protein expression and purification

All constructs were transformed into BL21-Star (DE3) cells (Invitrogen) containing the pRIL plasmid isolated from BL21-CodonPlus-RIL cells (Agilent) and plasmid pRK586 encoding the Tobacco Etch Virus (TEV) protease as described.[17] These cells produce a protein product

fused to an amino-terminal hexahistidine tag. 2L of TB media containing ampicillin, kanamycin, and chloramphenicol were inoculated with an overnight culture for an initial OD_{600} of approximately 0.1. The cells were grown to mid log phase at 37ºC and then the temperature was reduced to 20ºC. Protein expression was induced with 0.4 mM Isopropyl β-D-1-thiogalactopyranoside (IPTG) and the cells were harvested after 10h. Purification was performed as described previously for full-length *Pf*LipL1.[14] Briefly, *Pf*LipL1 variants were purified by immobilized metal ion chromatography followed by cation exchange chromatography and gel filtration chromatography. The first two steps of purification were performed on the same day to avoid proteolytic cleavage. Purified *Pf*LipL1 mutants were concentrated to approximately 5 $mg \cdot mL^{-1}$ and stored at -80ºC.

Protein crystallization and data collection

Lipoyl-*Pf*LipL1$_{\Delta 243\text{-}279}$ complex was prepared by adding 1.2 mol equiv of lipoate and excess ATP to 5 $mg \cdot mL^{-1}$ apo-LipL1$_{\Delta 243\text{-}279}$. Original crystals were obtained from a screen set up with 200 nL of protein and 200 nL reservoir containing 100 mM HEPES, pH 7.0 and 1.5 M $(NH_4)_2SO_4$ using a Mosquito crystallization robot (TTP Labtech) and equilibrated at 20 ºC in a 96-well sitting drop Intelli-Plate® (Art Robbins Instruments). The crystallization condition was further optimized to obtain larger crystals with 1 µL protein and 1 µL reservoir containing 100 mM HEPES, pH 7.0, 1.5 M $(NH_4)_2SO_4$, and 20% ethylene glycol and equilibrated at 20ºC on a 24-4 sitting drop Intelli-Plate® (Art Robbins Instruments). Crystals were mounted on a 0.2 mm cryoloop (Hampton Research) and flash frozen in liquid nitrogen for data collection. Data sets were collected at SSRL beam line 7-1 at 100K and λ 1.127085 Å.

Structure determination

The crystals belonged to the $P3_221$ space group with cell dimensions of a = b = 120.24 Å, c = 134.92 Å, α = β = 90°, and γ = 120°. Data reduction and scaling were performed with XDS/XSCALE.[18-20] The molecular replacement solution was obtained using alanine-substituted *E. coli* LplA (*Ec*LplA; PDB: 3A7A, chain A) N-terminal domain and C-terminal domain search models with the Phaser-MR module in PHENIX.[21,22] Model building was performed in Coot [23] and refinement in PHENIX. Lipoate-bound *Pf*LipL1$_{\Delta 243\text{-}279}$ was refined to a crystallographic R_{work} of 27.3% and an R_{free} of 30.2%. the final structure was analyzed with validation tools in MOLPROBITY.[24,25] Protein sequence similarity and Z-scores were calculated using the Dali server.[26] Sequence alignments were performed using the Clustal algorithm in Jalview.[27-29] Structural visualization was performed via PyMol.[30]

In vitro lipoylation assay

Lipoylation assays were performed as previously described.[14] Briefly, purified *Pf*LipL1 variants (1 μM) were incubated in reaction buffer (100 mM Na/K phosphate at pH 7.5 and 150 mM NaCl) containing 2 mM ATP, 2 mM $MgCl_2$, 200 μM *R*-lipoic acid, and 10 μM H-protein. After a 1-hour incubation at 37ºC reactions were quenched with the addition of gel loading buffer and analyzed by Western blot. The SDS-PAGE gel was transferred to a nitrocellulose membrane, blocked with 5% milk in PBS for 30 min, and probed with 1:5000 rabbit polyclonal α-LA (Calbiochem) for 2 h in 1% milk/PBS at room temperature. The membrane was washed with PBS three times and then probed with 1:5000 donkey α-Rabbit IgG horseradish peroxidase (HRP) secondary antibody (GE Healthcare) in 1% milk/PBS overnight at 4°C. The membranes were visualized with ECL western substrate (Pierce) and exposed to film.

Cell-based lipoylation assay

Cell based lipoylation was performed as previously described.[14] Briefly, lipoylation

deficient *E. coli* strain JEG3 containing the pRIL plasmid was transformed with a plasmid containing the candidate lipoate ligase (pMALcHT-*Pf*LipL1, pMALcHT-*Pf*LipL1$_{\Delta 259\text{-}269}$, pMALcHT-*Pf*LipL1$_{\Delta 254\text{-}274}$, pMALcHT-*Pf*LipL1$_{\Delta 249\text{-}279}$, or pMALcHT-*Pf*LipL1$_{\Delta 243\text{-}279}$). Cells were subsequently grown in LB medium with 1% glucose, 5 mM sodium succinate, 5 mM sodium acetate, 35 μg ·mL^{-1} chloramphenicol, 100 μg ·mL^{-1} ampicillin, and 200 μM *R*-lipoic acid. 20 mL cultures were grown to mid-log phase at 37ºC and induced with 0.4 mM IPTG for 10 h at 20ºC. Cells were harvested by centrifugation and re-suspended with 0.5 mL of buffer containing 20 mM HEPES, 100 mM NaCl at pH 7.5 and lysed by sonication. Cell lysates were clarified by centrifugation at 16 000 *g* and the supernatants were collected and resolved by SDS-PAGE (Invitrogen). Lipoylated proteins were visualized by Western blot as described above.

Accession code

The atomic coordinates and structure factors have been deposited in the Protein Data Bank as entry 5T8U

Results & Discussion

Overall Structure

To further our understanding into the lipoylation mechanism in malaria parasite mitochondria, we crystallized *Pf*LipL1$_{\Delta 243\text{-}279}$ in the presence of lipoate and excess ATP. The resulting crystals only contained lipoate bound in the active site presumably due to degradation of the lipoyl-AMP conjugate during the process of crystallization or trapping of the lipoyl-bound form in the crystal lattice. Lipoate-bound *Pf*LipL1$_{\Delta 243\text{-}279}$ crystallized in the trigonal $P3_221$ space group and has cell dimensions of a = b = 120.24 Å, c = 134.92 Å, α = β = 90°, and γ = 120° with two monomers per asymmetric unit. The structure was solved using an alanine-substituted model of *Ec*LplA (PDB code 3A7A, chain A). The N-terminal domain (residues 1-243) and C-terminal

domain (residues 250-337) were used as independent search models. Lipoyl-*Pf*LipL1$_{\Delta 243\text{-}279}$ was refined to 2.3 Å resolution with an R_{work} of 27.28% and an R_{free} of 30.16%. The crystallographic data and refinement statistics are summarized in Table 1. The R_{free} value is high given the resolution but after multiple rounds of refinement taking into account various factors, such as restraints and B-factors, it was not possible to obtain a lower R_{free} value. Analysis of the data with PHENIX Xtriage and POINTLESS do not suggest contributions from twinning or translational non-crystallographic symmetry. Furthermore, analysis with ZANUDA in CCP4 is consistent with the $P3_221$ space group used in this study. [31] Thus, we hypothesize that the high R_{free} value may be due a small but significant amount of degradation that is observed during the purification process.

The lipoate-bound *Pf*LipL1$_{\Delta 243\text{-}279}$ structure (Fig 1A) consists of a large N-terminal domain (NTD, residues 21-276), a linker region lacking defined secondary structure (residues 277-289), and a small C-terminal domain (CTD, residues 290-370). The NTD contains two β-sheets, a large mixed β -sheet made up of seven β -strands (β1, β2, β6, β7, β8, β9, and β10) and a small mixed-sheet made up of three strands (β3, β4, and β5). There are six α-helical elements surrounding the β-sheets (α1-6). The CTD consists of one anti-parallel β-sheet made up of three strands (β11, β12, and β13) and three α-helices (α7, α8, and α9). The two monomers in the asymmetric unit are in similar conformations and superimpose with a root-mean-square deviation (r.m.s.d.) of 0.4 Å for the corresponding 269 Cα atoms (Fig 1B). The most notable differences between the two monomers are a lack of density in Chain B residues 242-247 (a flexible loop at the site of the deletion) and an extension of the Chain B adenylate-binding loop at residues 194-200. The latter extension forms a β-strand with a symmetry related monomer.

Figure 1C shows a LIDIA diagram of the lipoate binding site in Chain A of the *Pf*LipL1$_{\Delta 243\text{-}279}$ structure.[32] Here, residues that are involved in hydrophobic interactions are shown in lime green and residues involved in H-bond interactions are shown as blue and green dashed lines for main chain and side chain interactions, respectively. It is important to note one additional difference between Chain A and Chain B in reference to the lipoate binding site. In Chain B it is the side chain of residue N152 as opposed to the amide hydrogen of residue G107 that forms the second hydrogen bond with the lipoate carboxylate.

Figures 1D and 1E show a close-up view of the lipoate binding pocket of *Pf*LipL1$_{\Delta 243\text{-}279}$ where residues that show significant interactions with the lipoate moiety are highlighted in stick representation and colored red (hydrophobic interactions) or blue (H-bond interactions). The pocket is defined by interactions with residues from β2, β5, β9, β10, and the loop region between β4 and β5, known as the lipoate-binding loop (residues 101-106). The lipoate binding loop is a hallmark of all lipoate protein ligases and lipoate transferases. It is of special interest to highlight the hydrogen bonding interaction between the lipoate carbonyl and residue K160. Lipoate ligase enzymes are characterized by having an active site lysine that forms hydrogen bonds with both lipoate and ATP orienting the carboxylate of lipoate for a nucleophilic attack on the α-phosphorus atom of ATP.[33] Indeed, an alanine substitution of K160 renders full-length *Pf*LipL1 unable to form lipoyl-AMP and abrogates lipoylation activity *in vitro*.[14]

Structure comparison

We searched for proteins with structural similarity to *Pf*LipL1$_{\Delta 243\text{-}279}$ using the Dali server.[26] Generally, the Dali server measures similarity by a sum-of-pairs method that results in a Dali-Z score. Structures with a Dali-Z- score above 2 are considered to have significant similarity and will usually be characterized as having similar folds. The top scoring result from

the Dali server for *Pf*LipL1$_{\Delta 243\text{-}279}$ is a computationally designed resorfurin ligase that was designed based on the *Ec*LplA scaffold (PDB: 4TVY, Z-score: 32.4).[34] Additionally, apo-, lipoate-bound, and lipoyl-AMP-bound *Ec*LplA structures also have a high Z-score in the Dali server results (PDBs: 1X2G, 1X2H, 3A7R; Z-scores: 31.1, 31.1, 30.5, respectively). A sequence alignment of *Pf*LipL1$_{\Delta 243\text{-}279}$ and *Ec*LplA shows all secondary structure elements to be conserved and a percentage identity of 29.8% (Fig. 2A).

The structure of lipoate-bound *Pf*LipL1$_{\Delta 243\text{-}279}$ is in the same "bent" conformation as the *Ec*LplA structure in the "unliganded" form (Fig 2B).[33,35] In this conformation the CTD is bent such that it obscures the putative H-protein binding site in a similar mechanism as that observed for *Ec*LplA.[33] This conformation is characterized by a hydrogen bond between the amide of G106 of the lipoate-binding loop and the carbonyl of C321 in the CTD. Additionally, there is a conserved salt-bridge between residues K79 in the NTD and D328 in the CTD. Similar interactions can also be observed in the *Ec*LplA structures in the "bent" conformation. Comparison of the lipoate-bound- *Pf*LipL1$_{\Delta 243\text{-}279}$ to lipoyl-AMP-bound *Ec*LplA (Fig 2C) shows that a large structural rearrangement must occur in *Pf*LipL1$_{\Delta 243\text{-}279}$ to accommodate H-protein for lipoylation.

_Pf_LipL1 deletion mutants are characterized by wild-type like lipoylation activity _in vitro_

Although full-length *Pf*LipL1 can be easily expressed and purified from *E. coli* with high yield, this construct is prone to spontaneous proteolytic cleavage. Amino acid sequencing revealed that cleavage initially occurs between K264 and E265 (data not shown); however, alanine substitution at position 264 does not prevent degradation even in the presence of protease inhibitors (data not shown). *Pf*LipL1 contains a low complexity region that is not conserved in other characterized lipoate ligases and despite the presence of this region in other *Plasmodium*

species there is no conservation of sequence or size. Full-length *Pf*LipL1 crystals can still be generated but only diffract to low resolution. We therefore decided to make a series of mutations that removed the low complexity sequence from our construct and tested the mutant *Pf*LipL1 constructs both in a cell-based lipoylation assay and an *in vitro* lipoylation assay. We made three different deletion mutants removing 5, 10 or 15 residues on both sides of K264 (deleting a total of 11, 21 or 31 amino acids, respectively). These constructs still suffered from degradation, prompting us to make a fourth deletion (*Pf*LipL1$_{\Delta 243\text{-}279}$) removing more residues from the low complexity loop. The latter construct, *Pf*LipL1$_{\Delta 243\text{-}279}$, shows minor degradation but is far more stable than the full-length construct. All loop deletion constructs appear to be enzymatically active. Indeed, *E. coli* substrate proteins are lipoylated when all *Pf*LipL1 variants are expressed in a lipoylation deficient cell line (**Fig S1A)**. Furthermore, *in vitro* lipoylation of the *Pf*H-protein, a canonical substrate enzyme, remains unchanged in the *Pf*LipL1$_{\Delta 243\text{-}279}$ deletion mutant (**Fig S1B)**. Since the lipoylation activity of all *Pf*LipL1 variants remains unchanged with deletion of the low complexity region the *Pf*LipL1$_{\Delta 243\text{-}279}$ construct is likely a good structural surrogate to understand the mechanism of lipoylation in *P. falciparum*.

Acknowledgements

Use of the Stanford Synchrotron Radiation Lightsource, SLAC National Accelerator Laboratory, is supported by the U.S. Department of Energy, Office of Science, Office of Basic Energy Sciences under Contract No.DE-AC02-76SF00515. The SSRL Structural Molecular Biology Program is supported by the DOE Office of Biological and Environmental Research, and by the National Institutes of Health, National Institute of General Medical Sciences (including P41GM103393). The contents of this publication are solely the responsibility of the

authors and do not necessarily represent the official views of NIGMS or NIH. The authors declare no conflict of interest.

Funding Information

This work was supported by the National Institutes of Health (R56 AI065853 and R01 AI125534 to STP, F32 AI110028 to AJG), the Johns Hopkins Malaria Research Institute, and the Bloomberg Family Foundation. The funding agencies had no role in the design, data collection, interpretation or the decision to submit this work for publication.

References

1. Mudhune SA, Okiro EA, Noor AM, Zurovac D, Juma E, Ochola SA, Snow RW. The clinical burden of malaria in Nairobi: a historical review and contemporary audit. Malaria journal. 2011;10:138.

2. Okiro EA, Al-Taiar A, Reyburn H, Idro R, Berkley JA, Snow RW. Age patterns of severe paediatric malaria and their relationship to Plasmodium falciparum transmission intensity. Malaria journal. 2009;8(1):4.

3. Okiro EA, Bitira D, Mbabazi G, Mpimbaza A, Alegana VA, Talisuna AO, Snow RW. Increasing malaria hospital admissions in Uganda between 1999 and 2009. BMC medicine. 2011;9(1):37.

4. Delves M, Plouffe D, Scheurer C, Meister S, Wittlin S, Winzeler EA, Sinden RE, Leroy D. The activities of current antimalarial drugs on the life cycle stages of Plasmodium: a comparative study with human and rodent parasites. Beeson JG, editor. PLoS medicine. 2012;9(2):e1001169.

5. Fidock DA, Eastman RT, Ward SA, Meshnick SR. Recent highlights in antimalarial drug resistance and chemotherapy research. Trends in Parasitology. 2008;24(12):537–544.

6. Dondorp AM, Fairhurst RM, Slutsker L, Macarthur JR, Breman JG, Guerin PJ, Wellems TE, Ringwald P, Newman RD, Plowe CV. The threat of artemisinin-resistant malaria. The New England journal of medicine. 2011;365(12):1073–1075.

7. Phyo AP, Nkhoma S, Stepniewska K, Ashley EA, Nair S, McGready R, ler Moo C, Al-Saai S, Dondorp AM, Lwin KM, et al. Emergence of artemisinin-resistant malaria on the western border of Thailand: a longitudinal study. Lancet (London, England). 2012;379(9830):1960–1966.

8. Allary M, Lu JZ, Zhu L, Prigge ST. Scavenging of the cofactor lipoate is essential for the survival of the malaria parasite Plasmodium falciparum. Mol Microbiol. 2007;63(5):1331–1344.

9. Spalding MD, Prigge ST. Lipoic acid metabolism in microbial pathogens. Microbiology and molecular biology reviews : MMBR. 2010;74(2):200–228.

10. Wrenger C, Müller S. The human malaria parasite Plasmodium falciparum has distinct organelle-specific lipoylation pathways. Mol Microbiol. 2004;53(1):103–113.

11. Foth BJ, Ralph SA, Tonkin CJ, Struck NS, Fraunholz M, Roos DS, Cowman AF, McFadden GI. Dissecting apicoplast targeting in the malaria parasite Plasmodium falciparum. Science. 2003;299(5607):705–708.

12. Falkard B, Kumar TRS, Hecht L-S, Matthews KA, Henrich PP, Gulati S, Lewis RE, Manary MJ, Winzeler EA, Sinnis P, et al. A key role for lipoic acid synthesis during Plasmodium liver stage development. Cellular microbiology. 2013;15(9):1585–1604.

13. Deschermeier C, Hecht L-S, Bach F, Rützel K, Stanway RR, Nagel A, Seeber F, Heussler VT. Mitochondrial lipoic acid scavenging is essential for Plasmodium berghei liver stage development. Cellular microbiology. 2012;14(3):416–430.

14. Afanador GA, Matthews KA, Bartee D, Gisselberg JE, Walters MS, Freel Meyers CL, Prigge ST. Redox-dependent lipoylation of mitochondrial proteins in Plasmodium falciparum. Mol Microbiol. 2014 Aug 13.

15. Spalding MD, Allary M, Gallagher JR, Prigge ST. Validation of a modified method for Bxb1 mycobacteriophage integrase-mediated recombination in Plasmodium falciparum by localization of the H-protein of the glycine cleavage complex to the mitochondrion. Molecular and Biochemical Parasitology. 2010;172(2):156–160.

16. Afanador GA, Guerra AJ, Swift RP, Rodriguez RE, Bartee D, Matthews KA, Schön A, Freire E, Freel Meyers CL, Prigge ST. A novel lipoate attachment enzyme is shared by Plasmodium and Chlamydia species. Submitted.

17. Muench SP, Rafferty JB, McLeod R, Rice DW, Prigge ST. Expression, purification and crystallization of the Plasmodium falciparum enoyl reductase. Acta Crystallographica Section D: Biological Crystallography. 2003;59(Pt 7):1246–1248.

18. Kabsch W. Automatic processing of rotation diffraction data from crystals of initially unknown symmetry and cell constants. Journal of Applied Crystallography. 1993;26(6):795–800.

19. Kabsch W. Integration, scaling, space-group assignment and post-refinement. Acta Crystallographica Section D: Biological Crystallography. 2010;66(2):133–144.

20. Kabsch W. XDS. Acta Crystallographica Section D: Biological Crystallography. 2010;66(2):125–132.

21. Adams PD, Afonine PV, Bunkóczi G, Chen VB, Davis IW, Echols N, Headd JJ, Hung LW,

Kapral GJ, Grosse-Kunstleve RW, et al. PHENIX: a comprehensive Python-based system for macromolecular structure solution. Acta Crystallographica Section D: Biological Crystallography. 2010;66(Pt 2):213–221.

22. McCoy AJ, Grosse-Kunstleve RW, Adams PD, Winn MD, Storoni LC, Read RJ. Phaser crystallographic software. Journal of Applied Crystallography. 2007;40(Pt 4):658–674.

23. Emsley P, Cowtan K. Coot: model-building tools for molecular graphics. Acta Crystallographica Section D: Biological Crystallography. 2004;60(Pt 12 Pt 1):2126–2132.

24. Chen VB, Arendall WB, Headd JJ, Keedy DA, Immormino RM, Kapral GJ, Murray LW, Richardson JS, Richardson DC. MolProbity: all-atom structure validation for macromolecular crystallography. Acta Crystallographica Section D: Biological Crystallography. 2010;66(Pt 1):12–21.

25. Davis IW, Leaver-Fay A, Chen VB, Block JN, Kapral GJ, Wang X, Murray LW, Arendall WB, Snoeyink J, Richardson JS, et al. MolProbity: all-atom contacts and structure validation for proteins and nucleic acids. Nucleic Acids Research. 2007;35(Web Server issue):W375–83.

26. Holm L, Rosenström P. Dali server: conservation mapping in 3D. Nucleic Acids Research. 2010;38(Web Server issue):W545–9.

27. Clamp M, Cuff J, Searle SM, Barton GJ. The Jalview Java alignment editor. Bioinformatics. 2004;20(3):426–427.

28. Waterhouse AM, Procter JB, Martin DMA, Clamp M, Barton GJ. Jalview Version 2--a multiple sequence alignment editor and analysis workbench. Bioinformatics. 2009;25(9):1189–1191.

29. Troshin PV, Procter JB, Barton GJ. Java bioinformatics analysis web services for multiple sequence alignment--JABAWS:MSA. Bioinformatics. 2011;27(14):2001–2002.

30. Schrödinger, LLC. The PyMOL Molecular Graphics System Version 1.8.

31. Lebedev AA, Isupov MN. Space-group and origin ambiguity in macromolecular structures with pseudo-symmetry and its treatment with the program Zanuda. Acta Crystallographica Section D: Biological Crystallography. 2014;70(Pt 9):2430–2443.

32. Emsley P. Tools for ligand validation in Coot. Acta crystallographica. Section D, Structural biology. 2017;73(Pt 3):203–210.

33. Fujiwara K, Maita N, Hosaka H, Okamura-Ikeda K, Nakagawa A, Taniguchi H. Global conformational change associated with the two-step reaction catalyzed by Escherichia coli lipoate-protein ligase A. Journal of Biological Chemistry. 2010;285(13):9971–9980.

34. Liu DS, Nivón LG, Richter F, Goldman PJ, Deerinck TJ, Yao JZ, Richardson D, Phipps WS, Ye AZ, Ellisman MH, et al. Computational design of a red fluorophore ligase for site-specific protein labeling in living cells. Proceedings of the National Academy of Sciences of the United

States of America. 2014;111(43):E4551–9.

35. Fujiwara K, Toma S, Okamura-Ikeda K, Motokawa Y, Nakagawa A, Taniguchi H. Crystal structure of lipoate-protein ligase A from Escherichia coli. Determination of the lipoic acid-binding site. Journal of Biological Chemistry. 2005;280(39):33645–33651.

36. Mosca R, Brannetti B, Schneider TR. Alignment of protein structures in the presence of domain motions. BMC Bioinformatics. 2008;9(1):352.

37. Mosca R, Schneider TR. RAPIDO: a web server for the alignment of protein structures in the presence of conformational changes. Nucleic Acids Research. 2008;36(Web Server issue):W42–6.

Figure Captions

Fig 1. Overall structure and binding pocket of lipoate-bound *Pf*LipL1$_{\Delta 243\text{-}279}$. (A) Cartoon representation of chain A of lipoate-bound *Pf*LipL1$_{\Delta 243\text{-}279}$. Secondary structure elements are labeled and the lipoate moiety is shown in stick representation. Important residues for the binding pocket are shaded in red and blue for residues contributing hydrophobic and H-bond interactions, respectively. (B) Superposition of chain A (cyan) and chain B (red) of lipoate-bound *Pf*LipL1$_{\Delta 243\text{-}279}$. The major differences in the two monomers are the lack of density for the loop defined by residues 242-247 and the extension of the adenylate-binding loop. (C) LIDIA representation of the binding site of Chain A. Residues involved in hydrophobic interactions are represented as lime green circles and residues involved in H-bond interactions are represented as blue or green dashed lines for main chain or side chain interactions, respectively. (D) and (E) surface representation of the lipoate binding pocket. Important residues are shown in stick representation and colored blue or red for or H-bonds or hydrophobic interactions, respectively. H-bonds are represented as blue dashed lines.

Fig 2 Comparison of *Pf*LipL1and *Ec*LplA. (A) Clustal sequence alignment of full-length *Pf*LipL1 and *Ec*LplA. Residues are colored using the ClustalX color scheme. Secondary structure elements are labeled as follows: arrows represent β-strands and rectangles represent α-helices. The lipoate-binding loop is highlighted with a grey-dashed line between β4 and β5 and the adenylate-binding loop is highlighted with a grey dashed line between and β10 and α5. The site of proteolytic cleavage in full length *Pf*LipL1 is marked with a red asterisk (B) Overlay of lipoate-bound *Pf*LipL1$_{\Delta 243\text{-}279}$, colored cyan, and lipoate bound *Ec*LplA (PDB 1X2H), colored

slate generated by the RAPIDO server.[36,37] Both structures are considered to be in the "bent" conformation which is incompatible with binding substrate proteins. (C) Overlay of lipoate-bound *Pf*LipL1$_{\Delta 243\text{-}279}$, colored cyan, and lipoyl-AMP bound *Ec*LplA (PDB 3A7R), colored salmon. The CTD of *Ec*LplA has translated approximately 90º and rotated approximately 180º to accommodate substrate enzyme binding. It is of interest to note the formation of a small β-strand in the CTD from residues that belong to the long adenylate-binding loop.

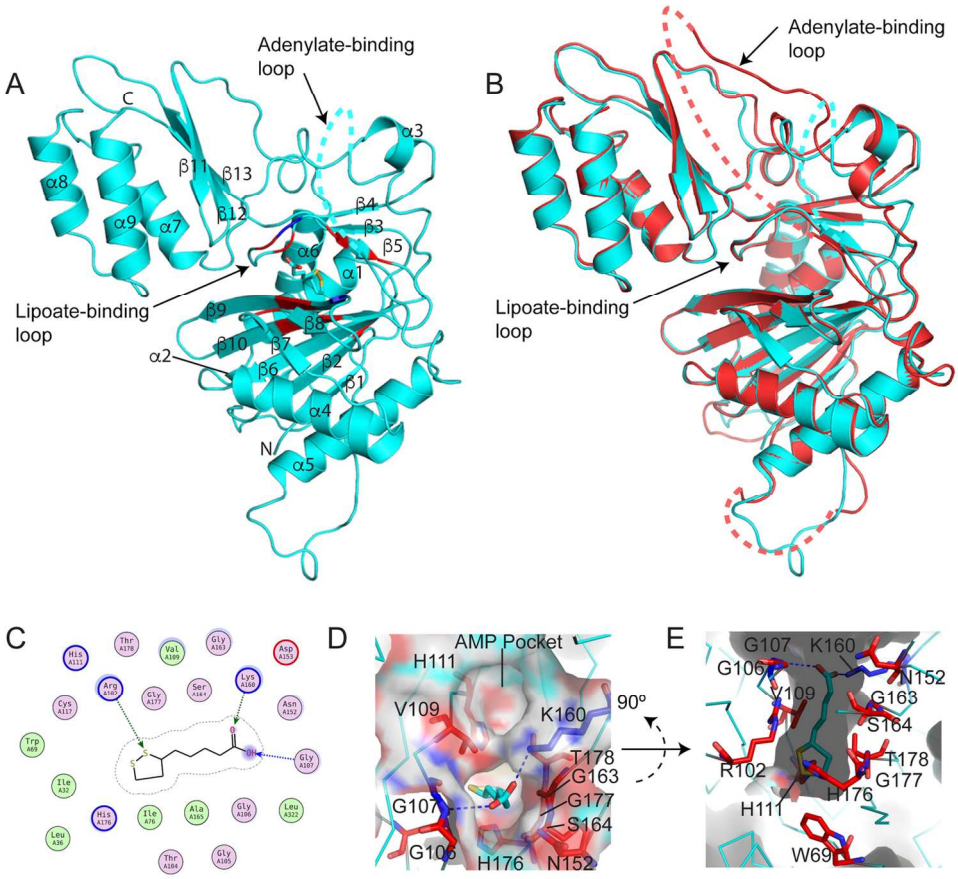

Fig 1. Overall structure and binding pocket of lipoate-bound PfLipL1Δ243-279. (A) Cartoon representation of chain A of lipoate-bound PfLipL1Δ243-279. Secondary structure elements are labeled and the lipoate moiety is shown in stick representation. Important residues for the binding pocket are shaded in red and blue for residues contributing hydrophobic and H-bond interactions, respectively. (B) Superposition of chain A (cyan) and chain B (red) of lipoate-bound PfLipL1Δ243-279. The major differences in the two monomers are the lack of density for the loop defined by residues 242-247 and the extension of the adenylate-binding loop. (C) LIDIA representation of the binding site of Chain A. Residues involved in hydrophobic interactions are represented as lime green circles and residues involved in H-bond interactions are represented as blue or green dashed lines for main chain or side chain interactions, respectively. (D) and (E) surface representation of the lipoate binding pocket. Important residues are shown in stick representation and colored blue or red for or H-bonds or hydrophobic interactions, respectively. H-bonds are represented as blue dashed lines.

137x123mm (300 x 300 DPI)

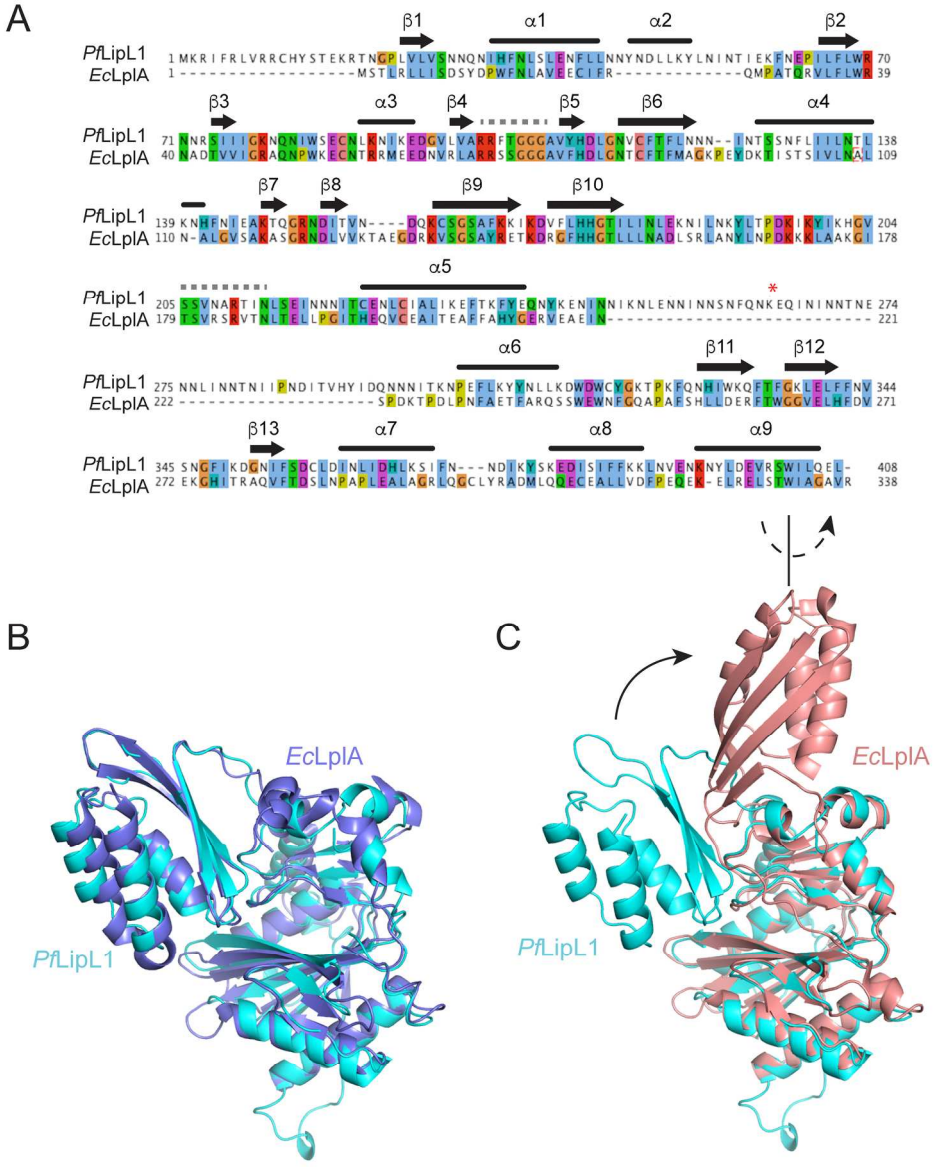

Fig 2 Comparison of PfLipL1and EcLplA. (A) Clustal sequence alignment of full-length PfLipL1 and EcLplA. Residues are colored using the ClustalX color scheme. Secondary structure elements are labeled as follows: arrows represent β-strands and rectangles represent α-helices. The lipoate-binding loop is highlighted with a grey-dashed line between β4 and β5 and the adenylate-binding loop is highlighted with a grey dashed line between and β10 and α5. The site of proteolytic cleavage in full length PfLipL1 is marked with a red asterisk (B) Overlay of lipoate-bound PfLipL1Δ243-279, colored cyan, and lipoate bound EcLplA (PDB 1X2H), colored slate generated by the RAPIDO server.35,36 Both structures are considered to be in the "bent" conformation which is incompatible with binding substrate proteins. (C) Overlay of lipoate-bound PfLipL1Δ243-279, colored cyan, and lipoyl-AMP bound EcLplA (PDB 3A7R), colored salmon. The CTD of EcLplA has translated approximately 90º and rotated approximately 180º to accommodate substrate enzyme binding. It is of interest to note the formation of a small β-strand in the CTD from residues that belong to the long adenylate-binding loop.

186x227mm (300 x 300 DPI)

Table 1. Data collection and refinement statistics for lipoate-bound *Pf*LipL1$_{\Delta 243\text{-}279}$

Data Collection	
Resolution range (Å)	44.97 - 2.32 (2.41 - 2.32)
Total reflections	289251 (28279)
Unique reflections	48819 (4399)
Multiplicity	5.9 (5.8)
Completeness (%)	96.5 (90.4)
Mean I/sigma(I)	9.9 (0.6)
R-merge	0.139 (2.672)
CC1/2	0.998 (0.491)
CC*	0.999 (0.812)
Wilson B-factor (Å^2)	53.07
Space group	P 3_2 2 1
Unit cell	
a, b, c (Å)	120.2, 120.2, 134.9
α, β, γ (º)	90, 90, 120
Refinement	
Reflections used in refinement	47298
Reflections used for R-free	2309
R-work (%)	27.28
R-free (%)	30.16
Molecules in asymmetric unit	2
Number of non-hydrogen atoms	5594
macromolecules	5486
ligands	24
solvent	84
Protein residues	671
Ramachandran favored / outliers	
total	624 / 1
(%)	95 / 0.15
Rotamer outliers (%)	0.33
Average B-factor (Å^2)	79.65
macromolecules (Å^2)	80.06
ligands (Å^2)	88.07
solvent (Å^2)	50.41
RMS bonds (Å) / angles (º)	0.002 / 0.47
RMSZ bonds / angles	0.24 / 0.42

Statistics for the highest-resolution shell are shown in parentheses.